Viscoplastic Matrix Materials for Embedded 3D Printing

Abigail K. Grosskopf,[†] Ryan L. Truby,[‡] Hyoungsoo Kim,[†,§] Antonio Perazzo,[†] Jennifer A. Lewis,*[‡] and Howard A. Stone*[†]

[†]Department of Mechanical and Aerospace Engineering, Princeton University, Princeton, New Jersey 08544, United States
[‡]John A. Paulson School of Engineering and Applied Sciences, Wyss Institute for Biologically Inspired Engineering, Harvard University, Cambridge, Massachusetts 02138, United States
[§]Department of Mechanical Engineering, KAIST, Daejeon 34141, South Korea

S Supporting Information
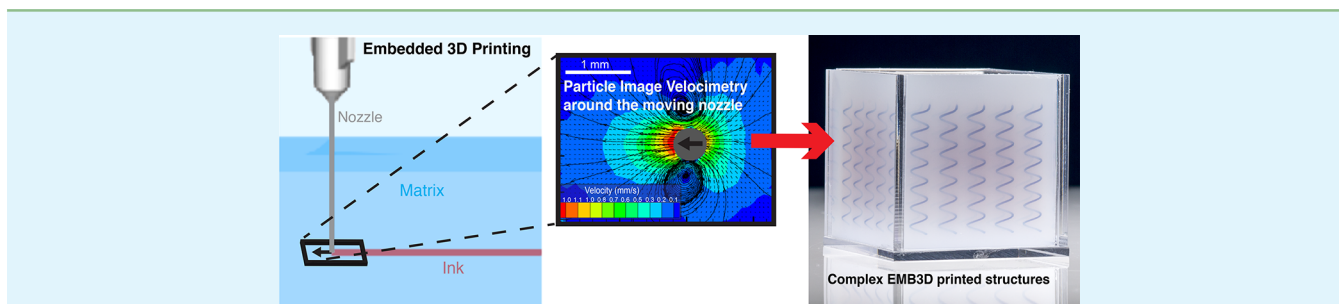
ABSTRACT: Embedded three-dimensional (EMB3D) printing is an emerging technique that enables free-form fabrication of complex architectures. In this approach, a nozzle is translated omnidirectionally within a soft matrix that surrounds and supports the patterned material. To optimize print fidelity, we have investigated the effects of matrix viscoplasticity on the EMB3D printing process. Specifically, we determine how matrix composition, print path and speed, and nozzle diameter affect the yielded region within the matrix. By characterizing the velocity and strain fields and analyzing the dimensions of the yielded regions, we determine that scaling relationships based on the Oldroyd number, Od, exist between these dimensions and the rheological properties of the matrix materials and printing parameters. Finally, we use EMB3D printing to create complex architectures within an elastomeric silicone matrix. Our methods and findings will both facilitate future characterization of viscoplastic matrices and motivate the development of new materials for EMB3D printing.

KEYWORDS: embedded three-dimensional printing, 3D printing, particle image velocimetry, rheology, viscoplasticity

1. INTRODUCTION

Three-dimensional (3D) printing is revolutionizing the design and manufacturing of soft matter with programmable composition, form, and function.[1] One emerging method, known as embedded 3D (EMB3D) printing, involves direct patterning of materials within soft supporting matrices along predefined omnidirectional printing paths (Figure 1). To date, this technique has been used to create 3D microvascular networks embedded in hydrogels,[2] soft sensors,[3] and other complex 3D structures,[4,5] including autonomous soft robots.[6] These architectures would be difficult to make solely by molding, casting, or other 3D printing methods.[7]

To enable EMB3D printing, the ink and matrix materials must meet several requirements.[1,3,6] First, the ink must be a shear-thinning yield stress fluid that controllably flows out of the print nozzle when a specified pressure is applied. Qualitatively, inks possess a shear elastic modulus, G'_{ink}, and yield stress, $\tau_{y,ink}$, that are approximately an order of magnitude larger than those of the matrix, G'_{matrix} and $\tau_{y,matrix}$, respectively, as reported previously.[3] When G'_{ink} is too large compared to G'_{matrix}, the translating nozzle can drag the ink within the matrix material. By contrast, when G'_{ink} is too low compared to G'_{matrix},

the ink filament can fragment and bead up.[3] The matrix materials must also consist of shear-thinning, yield stress fluids, which possess a sufficiently high G'_{matrix} to support the printed structures and a $\tau_{y,matrix}$ that is low enough to allow the translating nozzle to move freely throughout the matrix. However, when $\tau_{y,matrix}$ is too low compared to the viscous stresses associated with nozzle displacement, the translating nozzle will create stress fields that yield and displace the printed features. Alternately, when $\tau_{y,matrix}$ is too large, crevices form behind the translating nozzle, leading to voids that must be filled through the introduction of a filler fluid on the top surface of the matrix.[2,3] Thixotropic matrix materials, that is, materials that exhibit a time-dependent rheological behavior because of dynamic restructuring at the microscale, mitigate crevice formation and hence obviate the use of a filler fluid during EMB3D printing. Furthermore, the ink and matrix materials should be chemically compatible and exhibit the desired composition and functionality required for the application of
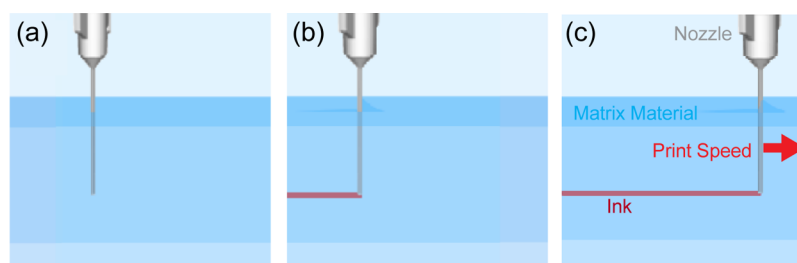
Figure 1. Schematic illustrations of EMB3D printing. (a) Print nozzle is lowered within a viscoplastic matrix, (b) ink is deposited into the matrix, and (c) nozzle is translated within the matrix at a given speed.

interest. To date, these requirements have been empirically determined through repetitive printing trials with the goal of optimizing the fidelity of the patterned features.[2,3,6]

To gain a fundamental understanding, we can model EMB3D printing by considering the flow of a viscoplastic matrix around a cylindrical nozzle. Specifically, we choose to treat the matrix material as a Herschel−Bulkley fluid

$$\boldsymbol{\tau} = \left(K |\dot{\boldsymbol{\gamma}}|^{n-1} + \frac{\tau_y}{\dot{\gamma}} \right) \dot{\boldsymbol{\gamma}} \quad \text{for } |\boldsymbol{\tau}| > \tau_y$$
$$\dot{\boldsymbol{\gamma}} = 0 \qquad\qquad\qquad \text{for } |\boldsymbol{\tau}| \leq \tau_y \qquad (1)$$

where $\boldsymbol{\tau}$ is the shear stress tensor, $\dot{\boldsymbol{\gamma}}$ is the strain rate tensor, τ_y is the yield stress, K is the consistency index, and n is the flow index.[8] The strain rate tensor is defined by

$$\dot{\boldsymbol{\gamma}} = \frac{1}{2}(\nabla \boldsymbol{v} + (\nabla \boldsymbol{v})^T) \qquad (2)$$

where $\boldsymbol{v}$ is the velocity field, ∇ is the gradient operator, and superscript T indicates the transpose of the tensor. We refer to the second invariant of the strain rate tensor as the shear rate, whose magnitude is given by

$$|\dot{\boldsymbol{\gamma}}| = \left[\frac{1}{2}(\dot{\boldsymbol{\gamma}} : \dot{\boldsymbol{\gamma}}) \right]^{1/2} = \left(\frac{1}{2} \dot{\gamma}_{ij} \dot{\gamma}_{ij} \right)^{1/2} \qquad (3)$$

where, for a two-dimensional flow, the indices i and j run from 1 to 2, and the summation convention is assumed.

The displacement of a sphere or a cylinder moving through a yield stress fluid has been studied through theory and simulations.[8−11] For example, Beris et al. modeled the movement of a sphere through a Bingham plastic and reaffirmed the idea of a "yield surface" around an object moving through a viscoplastic material.[10] The Oldroyd number (Od), the ratio of the material yield stress to the viscous stresses in a flow, is the most useful parameter to characterize the dimensions of the yielded areas of a Herschel−Bulkley fluid flowing around a cylinder

$$Od = \frac{\tau_y d^n}{K U^n} \qquad (4)$$

where U is the print speed of the translating nozzle, d is the nozzle outer diameter, and K, n, and τ_y are given by the Herschel−Bulkley eq 1.[8,9] For these fluids, the Reynolds number, the ratio of inertial to viscous forces in a flow, is defined as

$$Re = \frac{\rho d^n U^{2-n}}{K} \qquad (5)$$

Prior experimental studies have used particle image velocimetry (PIV) to investigate the low Re and Od flows of nonthixotropic yield stress fluids, such as Carbopol and Laponite suspensions, around rigid objects.[12,13] Notably, Carbopol, a microgel based on covalently cross-linked poly-(acrylic acid) networks,[8,12] has been recently used as a matrix material for EMB3D printing.[4,5] These studies revealed that both Od and $\tau_{y,\text{matrix}}$ are key determinants in controlling the size of the yielded fluid envelope around rigid objects. However, few experimental studies have been carried out on thixotropic fluids because of the added complexity that arises from their time-dependent behavior, even though the complex yielding behavior of the viscoplastic matrix materials used in EMB3D printing plays an important role in determining the quality of patterned structures.

Here, we investigate how viscoplastic matrix materials used in EMB3D printing[6] yield using rheological analysis combined with PIV. Specifically, we explore how matrix composition, print speed, and nozzle diameter influence the region of the matrix yielding around the nozzle during printing. By characterizing the velocity and strain fields and analyzing the dimensions of the yielded regions, we determine that scaling relationships based on the Od exist between these dimensions and the matrix rheology and printing parameters. The relationships corroborate general observations noted during EMB3D printing. Our methods and findings lend themselves to a deeper understanding of the viscoplastic matrix material behavior during EMB3D printing and serve as a rheological rubric to inform selection of the matrix and print parameters for improved EMB3D printing. These insights will inform future functional matrix material designs as well as strategies for print path optimization to improve the overall print fidelity and complexity that is possible with EMB3D printing.

2. EXPERIMENTAL SECTION

2.1. Matrix Materials. We used matrix materials composed of mixtures of two types of polydimethylsiloxane (PDMS), Sylgard 184 and SE 1700 (which contains approximately 20 wt % fumed silica). Fumed silica nanoparticles consist of branched, chain-like, 3D secondary particles that cluster into tertiary particles. Fumed silica particles act as a rheological modifier that imparts an appropriate elastic modulus G'_{matrix} and yield stress $\tau_{y,\text{matrix}}$. Individual fumed silica particles are approximately spherical and on the order of 20 nm in diameter. Within a critical concentration range, the fumed silica mixed into PDMS (SE 1700, Dow Corning, Inc.) can impart a thixotropic behavior.[15] Platinum-based catalysts are added to the resulting matrices before printing. Under ambient conditions, the matrix materials begin to partially cross-link and increase in viscosity after approximately one hour, and EMB3D printing must be performed within this "pot life". For the PIV study, we added silicone oil of identical viscosity in place of the catalyst solution to these PDMS-
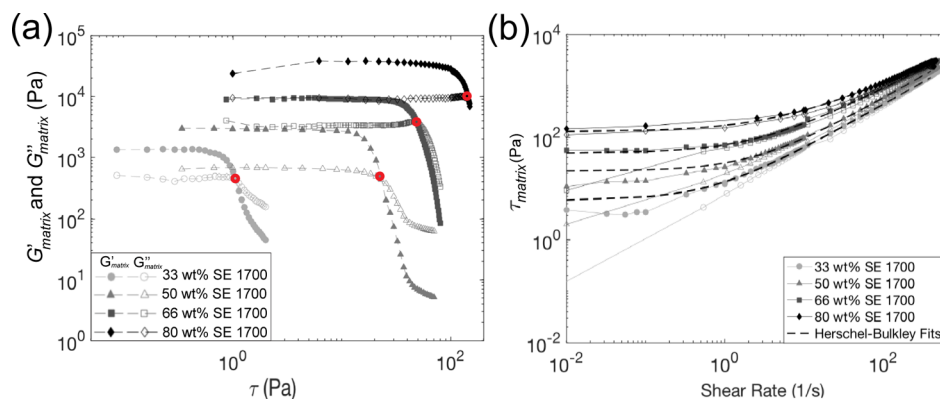
Figure 2. (a) Elastic, G'_{matrix}, and viscous, G''_{matrix}, moduli as a function of the oscillatory shear stress, τ, for fumed silica-filled PDMS matrix materials consisting of different SE 1700 content (wt %) at a frequency of 1 Hz. Amplitude sweeps are performed to determine yield stress values, $\tau_{y,matrix}$, which are circled in red for each fumed silica ratio. (b) Shear stress, τ, as a function of the shear rate. Flow sweeps and ramps are performed for all matrix materials. Closed symbols represent steady-state sweeps with an increasing shear rate. Open symbols represent steady-state ramps with a decreasing shear rate. Dashed lines indicate predictions of the Herschel−Bulkley model (eqs 1−3).

based matrices to prevent cross-linking. In this case, PIV experiments could be carried out for several hours.

2.2. EMB3D Printing. An EMB3D printing demonstration is conducted to demonstrate the consequences of matrix material yielding on the final print results. A representative ink composed of 25 wt % Pluronic F127 (Pluronic, Sigma-Aldrich) in deionized water is used. At room temperature, this ink exhibits a shear-thinning behavior,[2] $\tau_{y,ink} \approx 150$ Pa, and $G'_{ink} > 10^4$ Pa. A 1:1 mass ratio of red to blue food coloring is added to the Pluronic ink to facilitate visualization. The ink is loaded at 2 °C into a 3 cm^3 syringe barrel (EFD Nordson), capped, and then degassed by centrifugation for 5 min before printing. The ink physically gels as it returns to room temperature during centrifugation. Printing demonstrations are conducted in matrix materials composed of SE 1700 contents of 33, 50, and 66 wt % using a custom 3D printer (ABG 10000, Aerotech Inc., Pittsburg, PA, USA).[6] All matrix materials are poured into Petri dishes or acrylic containers and degassed under vacuum before printing. The Pluronic ink is extruded through 12.7 mm long, 25 gauge print nozzles with inner and outer diameters of 0.25 and 0.52 mm, respectively (EFD Nordson). The ink is extruded with pressures of 30 and 25 psi when printed at 2 and 0.5 mm/s, respectively.

2.3. Rheological Measurements. A stress-controlled rheometer (Anton Paar Physica MCR 301) equipped with cone and plate geometry (50 mm diameter) with an angle $\beta = 1°$ is used for rheological studies. The gap at the truncated tip was set at 0.049 mm for all tests. Oscillatory shear rheometry tests are performed at a frequency of 1 Hz.

2.4. PIV and Image Analysis. To visualize the flow field with PIV, a solution of fluorescent particles (Polysciences, Inc.) (5.68×10^9 particles/mL) is added at a volume fraction of polystyrene particles of 0.0015. At this solid loading, the matrix rheology is not adversely modified, and experimental results are reproducible. A glass dish is then filled with 12 g of each fluorescent particle-laden matrix material prior to carrying out the PIV measurements. To image during the print nozzle translation, an apparatus was built to extend over the microscope (Leica DMI6000, inverted fluorescent microscope). A 1D motion controller (Thorlabs) was attached to a post and suspended over the microscope.

The average background noise is first subtracted from all PIV images, and image intensities are scaled on a range from 0 to 1. A Gaussian filter is then applied to each image. The velocity vectors are obtained by applying 2D cross-correlations of the particle distribution with multiple interrogation windows of 64 × 64 pixels with 50% overlap for the coarse grid and 32 × 32 pixels with 50% overlap for the refined grid system. The random error associated with the PIV measurement is 0.05 pixel units for the given interrogation domain.[17,18] Our frame of reference and resolution consisted of approximately 125 pixels/mm. The optimal frame steps within this

group of images are chosen in relation to the displacement of the nozzle diameter to keep the mean particle displacement within the range of 5 to 15 pixels for all tests.[19] The concentration of the fluorescent particles is optimized, so that approximately 5 particles are present in each interrogation window, which is a recommended heuristic used in PIV.[19] Stokes numbers $\left[\left(St = \frac{t_0 U}{d} \right), \text{ where } t_0 = \frac{\rho_p d_p^2}{18 \mu_g}, \right.$ U is the print speed, d is the nozzle outer diameter, ρ_p is the density, d_p is the particle diameter, and μ_g is the dynamic viscosity of the matrix material] for our PIV experiments are approximately 10^{-14}; therefore, particles can be assumed to follow the fluid motion almost perfectly.[18] All image processing procedures are performed in Matlab (Figure S1).

To determine the dimensions of the yielded regions around the translating nozzle, a Matlab code was written to scan experimental shear rate fields. The boundary of the yielded region is defined as the first coordinate scanning outward from the center of the nozzle in the PIV grid that first fell below the noise level threshold for a given speed. Both the dimensions perpendicular to and in front of the nozzle are examined. Background noise becomes more significant in the shear rate fields because of the derivatives present in the tensor definition compared to the velocity field. The background noise level in the shear rate calculation is highly dependent on the number of images skipped during the PIV algorithm.

3. RESULTS

3.1. Matrix Rheology. The rheology of matrix materials composed of mixtures of PDMS materials, that is, Sylgard 184 and SE 1700, a fumed silica-filled PDMS (approximately 20 wt % fumed silica), is investigated with 33 wt % SE 1700, 50 wt % SE 1700, 66 wt % SE 1700, and 80 wt % SE 1700. These elastomeric matrices have been used previously for EMB3D printing of soft sensors and robots.[6] To determine the yield stress of each matrix, oscillatory shear rheometry tests are performed at a frequency of 1 Hz (Figure 2a). There is a gradual decrease in G'_{matrix} and G''_{matrix} close to the yield stress, indicating that yielding is not a sharp transition for these materials.[14] There are two primary methods to identify the point of yielding: one is to identify the yield point where G'_{matrix} starts to decrease before it crosses G''_{matrix}[14] and the other is to use the shear stress value at which there is a crossover of G'_{matrix} and G''_{matrix} as $\tau_{y,matrix}$. For our analysis, we use the latter value and find that the yield stress increases with increasing SE 1700 content (Figure 2a).

To observe the thixotropic behavior and obtain the Herschel−Bulkley parameters for each matrix material,

continuous shear flow tests with the shear rate increasing and tests with the shear rate decreasing are also performed (Figure 2b). A quantitative analysis of this behavior is provided in Figure S9. A nonlinear regression is carried out on the flow sweep data to determine the Herschel−Bulkley parameters for each matrix material (Table 1). At low shear rates, the matrix

Table 1. Summary of Rheological Parameters for all Matrix Materials[a]

SE 1700 (wt %)	$\tau_{y,matrix}$ (Pa)	G'_{matrix} (Pa)	$\tau_{y,matrix}$(HB) (Pa)	K	n
33	1.3 ± 3	8.1	4.0 ± 2	8.3 ± 1	0.88 ± 0.1
50	18.4 ± 5	92.5	19.9 ± 2	9.7 ± 1	0.86 ± 0.1
66	48.2 ± 6	390.7	48.4 ± 5	22.1 ± 1	0.79 ± 0.1
80	123.7 ± 14	515.3	127.3 ± 16	42.3 ± 6	0.69 ± 0.1

[a]Errors are reported with 95% confidence.

materials with lower SE 1700 (and fumed silica content) breakdown and the restructuring of the percolated fumed silica networks result in the hysteretic behavior of the matrix material, leading to deviations from the Herschel−Bulkley description under these conditions. Nevertheless, the yield stresses calculated from the Herschel−Bulkley fits are close to those

determined from the amplitude sweeps (Figure 2b, Table 1). Both the consistency index K and the flow index n increase with SE 1700 content, and hence with the amount of fumed silica, which is in good agreement with recently reported observations.[15]

3.2. EMB3D Printing. A simple 3D form is EMB3D-printed to illustrate the implications of matrix material composition and printing parameters on the fidelity of the features patterned within these matrices. For this demonstration, we used one ink (25 wt % Pluronic), one print nozzle (d = 0.52 mm), two print speeds (U = 0.5 and 2 mm/s), and three elastomeric matrices that represent a subset of those studied, that is, 33, 50, and 66 wt % SE 1700 formulations. Pluronic F127 is a triblock copolymer composed of poly(ethylene oxide)-*b*-poly-(propylene oxide)-*b*-poly(ethylene oxide), which is a commonly used fugitive ink for EMB3D printing.[6] This simple 3D form (Figure 3a) is printed within the three matrices using the four print paths shown in Figure 3b−d. The images of the patterned features reveal how matrix yielding impacts their fidelity (Figure 3e).Comparing these results, we find that matrix composition plays a critical role in enabling patterns that most closely resemble the desired 3D form in Figure 3a. The features printed with the 33 wt % SE 1700 matrix exhibit the most pronounced deviation from the intended form, while those
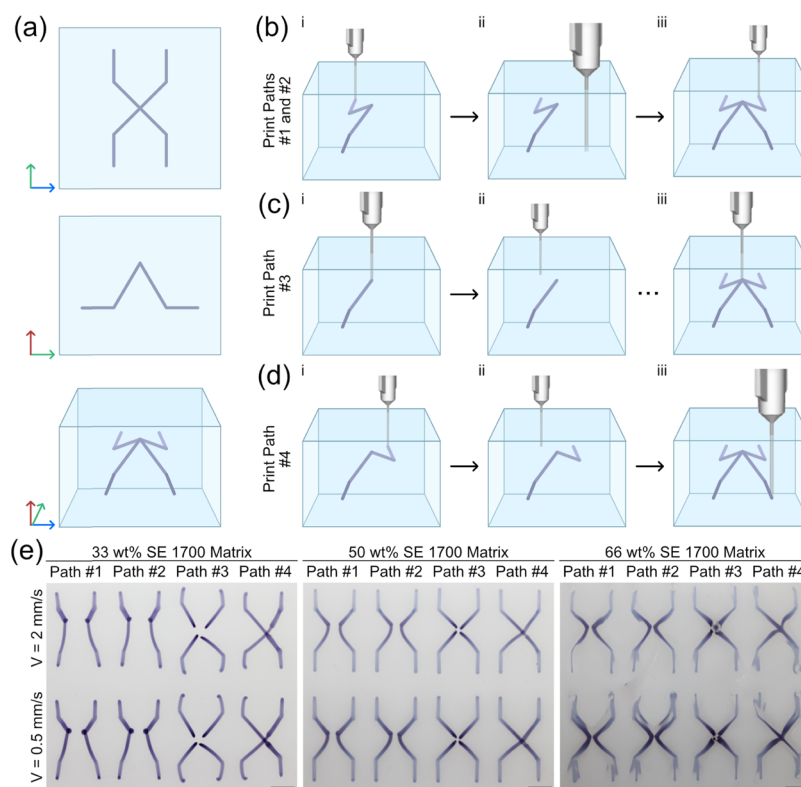

Figure 3. Matrix composition and print path effects on fidelity. (a) Top-down (top), side-on (middle), and 3D (bottom) views of a simple form that is EMB3D-printed. The blue, green, and red arrows to the left represent the *X*-, *Y*-, and *Z*-axes, respectively. (b−d). Schematic illustrations of print paths #1 through #4. For paths #1 and #2, the form is printed in halves: (i) left half of the form is printed, and the nozzle is raised out of the matrix and (ii) brought to the next start location, and (iii) right half of the form is printed. Paths #1 and #2 differ in that in path #2, a 5 min pause in printing is inserted before step (ii). (c) For path #3, the form is printed in four segments (i) with each segment terminating at the vertex. (ii) Printing continues in a clockwise fashion until (iii) the last segment is printed. (d) For path #4, the form is printed again in halves, but in a fashion to minimize ink displacement. (i) Bottom left and top right segments are first printed in one continuous filament, (ii) tip is brought to the next location, and (iii) top left and bottom right segments are printed in one continuous filament. (e) Results of printing the form with each print path in 33 wt % (left), 50 wt % (middle), and 66 wt % (right) SE 1700 matrices with each print path are shown for two print speeds, *U* = 2 mm/s (top row) and 0.5 mm/s (bottom row). (Nozzle *d* = 0.52 mm; scale bars = 3 mm.)

printed in the 66 wt % SE 1700 matrix most closely followed it (Figure 3e). As the least thixotropic of the three matrices, the 66 wt % SE 1700 matrix gave rise to small crevices and raised peaks during EMB3D printing, and the sample had to be rotated to better visualize the results (Figure S10).

The results in Figure 3e also indicate that print path selection influences pattern fidelity. Independent of matrix composition, we find that the printed 3D form exhibits the closest resemblance to the desired form using print path #4, with the greatest deviations observed using print paths #1 and #2. In paths #1 and #2, the embedded form is printed in halves with or without a 5 min delay between each half, respectively (Figure 3b), and matrix material yielding in front of the nozzle causes the deposited ink to be dragged downward when the nozzle is translated away from the vertex. At slower print speeds, the separation distance between the two halves at the intended vertex slightly decreases. Because thixotropic matrices recover their yield stress over time after yielding, path #2 is used to explore the effects of the 5 min recovery period on the final print results. However, no obvious difference in the printing fidelity was observed between paths #1 and #2 (Figure 3e). In path #3 (Figure 3c), the 3D form is printed in four continuous segments in a clockwise fashion, with each segment terminating in the center of the form at the intended vertex. Once a segment is printed, the nozzle is translated upward in the Z-direction and out of the matrix material. While the desired form is still not achieved with path #3, it does have improved fidelity compared to structures printed using paths #1 and #2. Slight discontinuities at the vertex arise because of modest lifting of the printed ink features when the nozzle is removed from the matrix material or neighboring segments are printed. Finally, in path #4 (Figure 3d), the form is printed in two diagonal halves. In the 50 and 66 wt % matrix formulations, path #4 clearly provides patterns that most closely resemble the intended form. The vertex is slightly off center because of ink displacement by the translating nozzle, but this displacement is small and could be diminished by slightly increasing the applied printing pressure. Selection of matrix material (i.e., selection of appropriate matrix material rheology), print speed, and print path all contribute to the final results in EMB3D printing.

3.3. Velocity Fields Generated During EMB3D Printing.
To better understand the abovementioned observations, we performed PIV experiments to investigate the effect of matrix composition, nozzle diameter, and print speed on matrix deformation. To determine the flow field around a moving nozzle using PIV, fluorescent polystyrene particles (2 μm diameter) are incorporated within the matrix materials. To simulate EMB3D printing, a simple printing apparatus composed of a one-dimensional motion controller that translates a nozzle within a given matrix of interest was constructed (Figure 4a). The inner and outer diameters of the three nozzles used are 0.15 and 0.31, 0.20 and 0.42, and 0.25 and 0.52 mm. The nozzle is lowered into the matrix material and held at a fixed distance of 2 mm from the bottom of the dish (Figure 4b) to minimize boundary effects arising from the stationary matrix–dish interface. To minimize the effects of matrix thixotropy, the PIV measurements are performed in 7 min intervals, which allow the matrix material to relax and restructure. In each test, the print nozzle moves from right to left in a different region of the matrix. The Od (eq 4) ranges from $Od = 0.1$ to 5, and the Reynolds number (eq 5) ranges from $Re = 10^{-6}$ to 10^{-4}. These parameters are calculated to characterize each experiment. Using this setup, we can readily
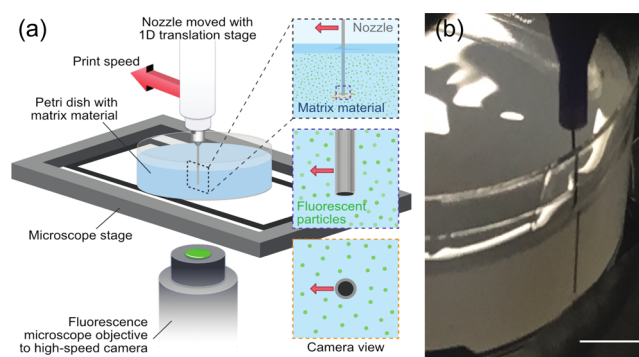

Figure 4. (a) Schematic view of the PIV experimental setup. A 1D motion-controlled stage equipped with a print nozzle attached is suspended over a fluorescent microscope. The nozzle is moved through the EMB3D printing matrix material, which contains fluorescent tracer particles. A high-speed camera is used to capture photos of the matrix immediately beneath the nozzle as it is translated through each matrix material. (b) Side view of a nozzle ($d = 0.31$ mm) in the plane of interest. The nozzle was kept at a 2 mm distance from the bottom of the Petri dish. Scale bar = 10 mm.

observe the deformation of the surrounding matrix in a horizontal plane at the bottom of the nozzle, as the nozzle translates through the matrix at a prescribed speed with a 5 μm/s accuracy.

The changes in the velocity flow field as the SE 1700 and fumed silica content within the matrix increase are shown in Figure 5. Each flow field uses a color scale to display the magnitude of the velocity, and streamlines are indicated. A region of significant vorticity appears near the nozzle, which becomes stronger with increasing SE 1700 content and fumed silica. Notably, this region is very weak in Newtonian fluids. The observed asymmetry in the velocity distribution in front of and behind the nozzle is reduced for matrices with the highest SE 1700 content (80 wt %), as shown in Figure 5d. As a control experiment, PIV experiments are also performed with Carbopol 940 as the matrix material (Figures S8 and S9).

The velocity profiles directly in front of and behind the nozzle are examined for all matrix materials and print speeds (Figure 6a). The dimensionless velocity profiles collapsed onto a master curve for each individual matrix material studied with characteristic velocity decays in front of and behind the nozzle. Arigo and McKinley[16] and Putz et al.[12] have suggested an exponential decay in front of the nozzle for shear-thinning yield stress fluids, which takes the form

$$\frac{u}{U} = e^{-r/fd} \tag{6}$$

where u is the local velocity, U is the print speed, r is the distance from the nozzle, d is the nozzle diameter, and f is a value characteristic of the Herschel–Bulkley fluid found from a regression of the data. The parameter f represents a dimensionless function of the nonlinear rheological parameters of the materials, most likely encompassing the yield stress, consistency index, and elastic modulus.[12,16] Exponential fits are performed for each matrix material on all nondimensional velocity profiles in front of (downstream) and behind the nozzle (upstream) to determine the exponent factor f for each decay. Figure 6a shows one set of representative tests of all matrix materials and the exponential fit for each matrix material. Each fit is performed using all of the collapsed data from 12 tests from each matrix material.
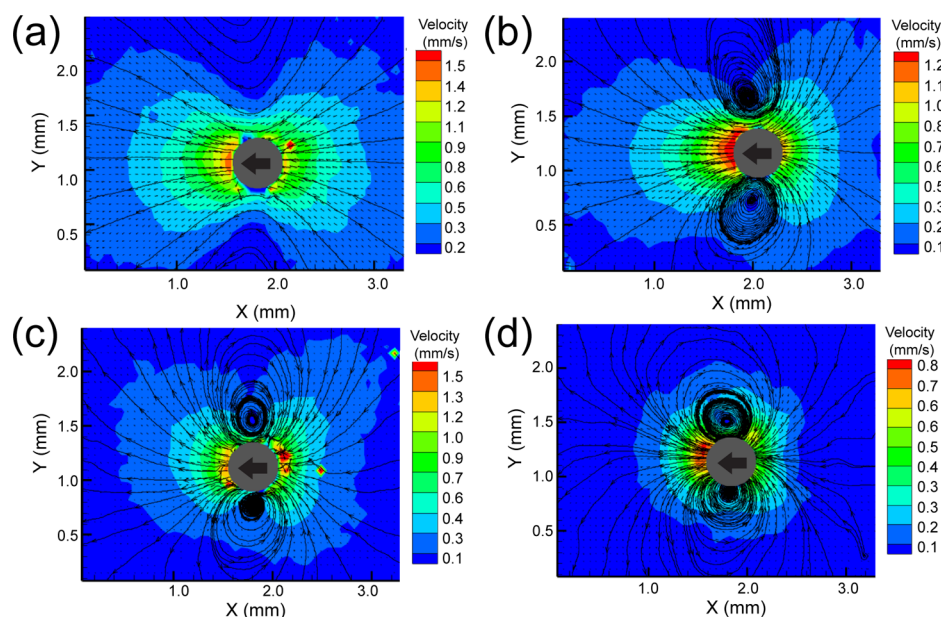
Figure 5. Velocity flow fields with streamlines within matrix materials of varying SE 1700 and fumed silica content using a nozzle (diameter = 0.52 mm) moving at 1.5 mm/s from right to left. (a) 33 wt % SE 1700, $Od = 0.2$, $Re = 1.1 \times 10^{-4}$. (b) 50 wt % SE 1700, $Od = 0.8$, $Re = 9.1 \times 10^{-5}$. (c) 66 wt % SE 1700, $Od = 0.9$, $Re = 4.4 \times 10^{-5}$. (d) 80 wt % SE1700, $Od = 1.5$, $Re = 2.6 \times 10^{-5}$.
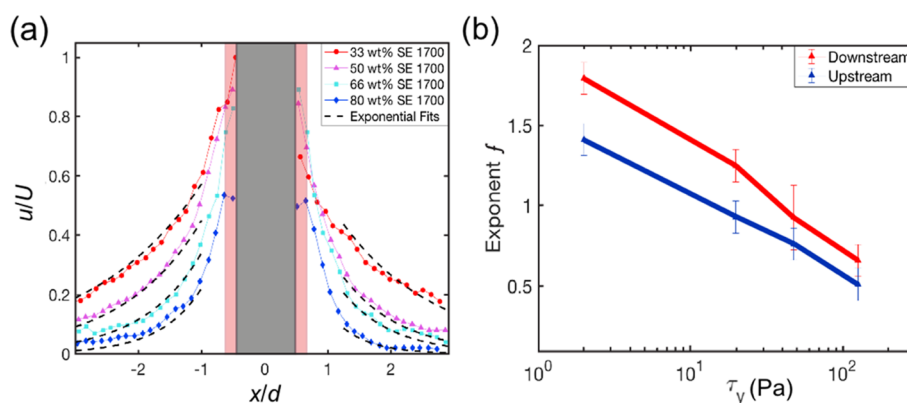

Figure 6. Effect of matrix composition on exponential decays of the velocity distribution in front of and behind the nozzle. (a) Gray region represents the nozzle area, and u is the measured matrix velocity at position x. Pink regions represent areas of lower PIV resolution close to the moving nozzle. Exponential decays downstream (left, in front of the nozzle) and upstream (right, behind the nozzle) of the nozzle for the four matrix materials for a $d = 0.42$ mm nozzle moving at $U = 1.5$ mm/s; the velocity distribution is fit using eq 6. The decay becomes more rapid with increased fumed silica content. (b) Fitted exponent f obtained from velocity profile decays (Table 2) as a function of material yield stress. The decay upstream of the nozzle is more rapid as shown by the lower exponents.

With increasing SE 1700 and fumed silica content, we observe faster exponential decays in velocity in front of the nozzle. However, changes in other parameters, such as the nozzle diameter and speed, do not affect the nondimensional decays. While matrices with higher SE 1700 content are more elastic (higher G'_{matrix} in dynamic conditions), their higher yield stress seems to dominate, leading to a faster decay (Figure 6b and Table 2).

3.4. Matrix Yielding During EMB3D Printing. While it is useful to understand the matrix response within the yielded region around the nozzle, it is most crucial for optimizing EMB3D printing to determine the boundary of the yielded region. As shown in Figure 3e, matrix deformation clearly results in the displacement of previously printed features and should be considered when optimizing the print path. While our observed exponential decays of the velocity profiles can help predict where the fluid velocity will be close to zero, this

Table 2. Exponential Decay Factors in Velocity Profiles for Fumed Silica-Filled PDMS Materials (eq 6)[a]

SE 1700 (wt %)	downstream f	upstream f
33	1.80 ± 0.1	1.41 ± 0.1
50	1.25 ± 0.1	0.93 ± 0.1
66	0.94 ± 0.2	0.76 ± 0.1
80	0.67 ± 0.1	0.51 ± 0.1

[a]Error is reported with 95% confidence.

analysis leads to extremely large dimensions for the yielded region. The term "yielded" is more traditionally defined in terms of the magnitude of the shear rate. Additionally, the fluctuations in velocity in the high vorticity regions make it difficult to analyze velocity profiles perpendicular to the direction of movement, and velocity gradient calculations account for such fluctuations.
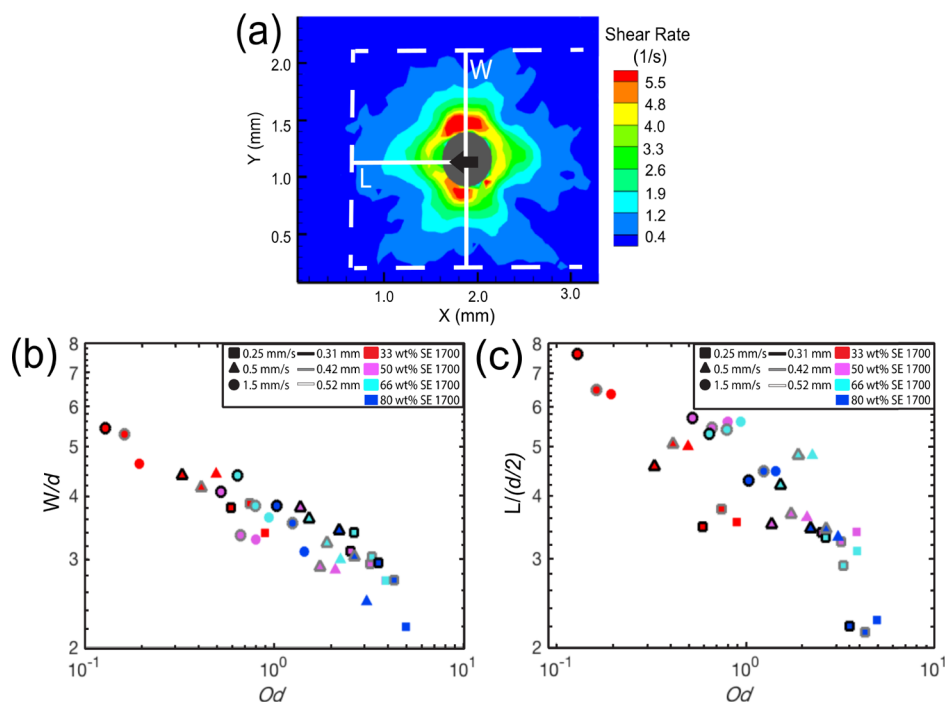
Figure 7. (a) Shear rate field with representative width W and length L measurement for the 50 wt % SE 1700 matrix with a nozzle diameter d = 0.52 mm and print speed U = 1.5 mm/s. The width W represents the maximum disturbed distance on both sides of the nozzle. The length L represents the maximum disturbed distance in front of the nozzle. (b) Nondimensional width (W/d) versus Od for various matrix compositions, nozzle diameters, and print speeds. Red symbols represent 33 wt %, magenta symbols represent 50 wt %, cyan symbols represent 66 wt %, and blue symbols represent 80 wt % SE 1700. Squares represent U = 0.25 mm/s, triangles represent U = 0.5 mm/s, and circles represent U = 1.5 mm/s. Black outlines represent d = 0.31 mm, gray outlines represent d = 0.42 mm, and no outlines represent d = 0.52 mm. (c) Nondimensional length $[L/(d/2)]$ versus Od for various matrix compositions, nozzle diameters, and print speeds. The matrix composition, print speed, and nozzle diameter correspond to the same symbol color, shape, and outline parameters as shown in (b).

To characterize the yielded region, the shear rate for all matrix compositions, nozzle diameters, and print speeds is calculated from the velocity fields according to

$$\dot{\gamma} = \left(\frac{1}{2}\right)^{1/2} (\dot{\gamma}_{xx}^{2} + \dot{\gamma}_{yy}^{2} + 2\dot{\gamma}_{xy}^{2})^{1/2} \tag{7}$$

where $\dot{\gamma}_{xx} = \frac{\partial v_x}{\partial x}$, $\dot{\gamma}_{yy} = \frac{\partial v_y}{\partial y}$, $\dot{\gamma}_{xy} = \frac{1}{2}\left(\frac{\partial v_x}{\partial y} + \frac{\partial v_y}{\partial x}\right)$ and $v_x(x,y)$ and $v_y(x,y)$ represent, respectively, the x and y velocity components. Velocity gradients are determined using numerical approximations on PIV data

$$\frac{\partial v_x}{\partial x} \approx \frac{\Delta v_x}{\Delta x}, \quad \frac{\partial v_y}{\partial y} \approx \frac{\Delta v_y}{\Delta y}, \quad \frac{\partial v_x}{\partial y} \approx \frac{\Delta v_x}{\Delta y}, \quad \frac{\partial v_y}{\partial x} \approx \frac{\Delta v_y}{\Delta x} \tag{8}$$

Because of limited PIV resolution and background noise in the PIV image analysis, the shear rate never reaches zero in our frame of reference. Background noise can have a significant effect on the data analysis and increases with increased print speed (Figures S2−S5). To determine a yielded region within these constraints, images of the quiescent matrix material are recorded and background noise levels are calculated for each nozzle velocity. Background noise did not significantly vary with matrix composition because the same fluorescent particle concentrations are added to each matrix. The determined noise levels are used as thresholds when measuring the yielded dimensions and normally represent approximately 8% of the maximum shear rate for a given test. These limitations lead to error associated with determining the dimensions of the yielded region.

A Matlab code was written to scan all experimental shear rate fields starting from the coordinates of the center of the nozzle to determine the dimensions of the yielded region (see the Experimental Section). An example of the computed shear rate fields and the yielded dimensions is provided in Figure 7a. The dimensions of the yielded material are most relevant for EMB3D printing. The measured dimensions are plotted against the Od for each matrix composition, print speed, and nozzle diameter investigated to determine how these parameters influence the yielded distance (Figure 7b,c). First, the entire width W of the yielded region perpendicular to the direction of the nozzle movement is measured for all conditions and nondimensionalized with the nozzle diameter. Figure 7b presents the effect of the Od on the nondimensional yielded width W/d, which ranges from 2× to 5× the nozzle diameter. The results confirm that the higher Od leads to smaller nondimensional yielded regions around the nozzle. According to this trend, when Od < 1, that is, for the 33 wt % SE 1700, the nondimensional width changes rapidly with changes in the Od. When Od > 1, that is, for the 80 wt % SE 1700, the nondimensional width of the yielded region changes less with changes in the Od, but crevices that develop behind the nozzle take a much longer time to heal. For the higher Od tests in Figure 7b, we observe a nearly constant level of scatter of approximately the diameter of the nozzle. Next, the length of the yielded region L in front of the nozzle is measured for all tests (Figure 7c). More scatter is observed when the nondimensional lengths are plotted against the Od, but a similar trend is apparent.

By varying printing parameters using the relationships presented above, we can fabricate complex architectures with EMB3D printing such as those presented in Figure 8. By calculating the Od for a given set of printing parameters, we can now estimate the dimensions of the yielded region around the nozzle.
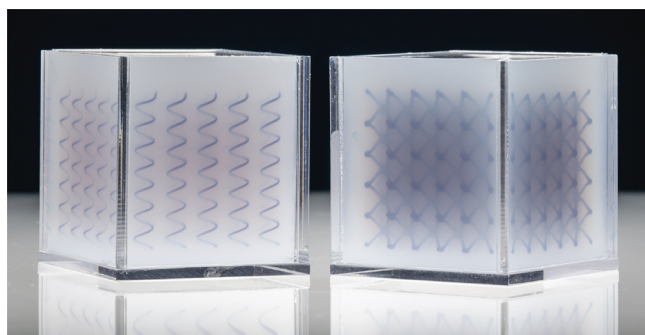

Figure 8. Optical image of EMB3D printed architectures, including an array of high aspect ratio spirals (left) and a body-centered cubic lattice (right), using the 25 wt % Pluronic ink (dark purple features) in a 50 wt % SE 1700 matrix with $d = 0.72$ mm and $U = 2$ mm/s ($Od = 0.83$). Acrylic cubes (5.1 cm edge length) contain the matrix during printing.

4. CONCLUSIONS

Our analysis connects dimensionless parameters to an emerging and impactful 3D printing technique and suggests that maximizing the Od is key to reducing the yielded dimensions around the nozzle during EMB3D printing. While tailoring the matrix rheology by changing its SE 1700 content is the most direct means of tuning the Od, the nozzle diameter and print speed also impact the Od. While other parameters, such as the Deborah number, are considered, the Od proved to be the most robust parameter for characterizing the yielded dimensions within a given matrix during EMB3D printing (Figures S6 and S7). Our PIV experiments corroborate the observations from our initial EMB3D printing demonstration, that is, that print fidelity increases with the increasing Od when a print path is selected that minimizes the previously patterned feature's exposure to matrix yielding around the translating nozzle. However, as the distortions observed for the 66 wt % SE 1700 matrix reveal (Figure 3e), choosing a more viscoplastic matrix that increases the Od for the highest fidelity printing may not ultimately be appropriate for EMB3D printing. In fact, it was not feasible to print within even stiffer matrices based on the 80 wt % SE 1700 matrix because of the formation of crevices. As such, suitable matrix materials for EMB3D printing must not only possess a high Od but also exhibit some thixotropic behavior that allows the matrix to "self heal" during the printing process.

In summary, we have systematically investigated the effects of elastomeric matrix composition and rheology, nozzle size, and print speed and path on EMB3D printing. We find that the 50 wt % SE 1700 matrix is well-suited for EMB3D printing because of its high $\tau_{y,matrix}$, $Od > 1$, and thixotropic behavior that allows crevices to "self heal" behind the translating nozzle. Our findings demonstrate a trend between the dimensions of the yielded region around a translating nozzle and the Od for the class of matrix materials studied here. While further studies are needed to elucidate whether such trends are universal, the insights gained can be used to optimize matrix rheology, inform printing parameter choices, aid print path design, and ultimately fabricate complex architectures of improved printing fidelity and complexity with EMB3D printing.

■ ASSOCIATED CONTENT

■ AUTHOR INFORMATION

Corresponding Authors

*E-mail: jalewis@harvard.seas.edu. Phone: (609) 258-9493. Fax: (609) 258-6109(J.A.L.).
*E-mail: hastone@princeton.edu (H.A.S.).

ORCID
Hyoungsoo Kim: 0000-0002-2393-723X
Jennifer A. Lewis: 0000-0002-0280-2774
Howard A. Stone: 0000-0002-9670-0639

Present Address
Department of Chemical Engineering, Stanford University, Stanford, CA 94305 (A.K.G.).

Author Contributions

A.K.G., R.L.T., J.A.L., and H.A.S. designed the research. A.K.G. performed rheology and PIV experiments. R.L.T. performed EMB3D printing demonstrations. H.K. helped to set up and analyze PIV experiments. A.P. helped to set up and analyze rheology experiments. All authors contributed toward writing the manuscript.

Notes

The authors declare the following competing financial interest(s): J.A.L. is a cofounder of Voxel8, Inc., a multimaterial 3D printing company.

■ ACKNOWLEDGMENTS

■ REFERENCES

(1) Truby, R. L.; Lewis, J. A. Printing soft matter in three dimensions. *Nature* **2012**, *540*, 371−378.
(2) Wu, W.; DeConinck, A.; Lewis, J. A. Omnidirectional printing of 3D microvascular networks. *Adv. Mater.* **2011**, *23*, H178−H183.
(3) Muth, J. T.; Vogt, D. M.; Truby, R. L.; Mengüç, Y.; Kolesky, D. B.; Wood, R. J.; Lewis, J. A. Embedded 3D printing of strain sensors within highly stretchable elastomers. *Adv. Mater.* **2014**, *26*, 6307−6312.

(4) Bhattacharjee, T.; Zehnder, S. M.; Rowe, K. G.; Jain, S.; Nixon, R. M.; Sawyer, W. G.; Angelini, T. E. Writing in the granular gel medium. *Sci. Adv.* **2015**, *1*, No. e1500655.

(5) Hinton, T. J.; Hudson, A.; Pusch, K.; Lee, A.; Feinberg, A. W. 3D printing PDMS elastomer in a hydrophilic support bath via freeform reversible embedding. *ACS Biomater. Sci. Eng.* **2016**, *2*, 1781−1786.

(6) Wehner, M.; Truby, R. L.; Fitzgerald, D. J.; Mosadegh, B.; Whitesides, G. M.; Lewis, J. A.; Wood, R. J. An integrated design and fabrication strategy for entirely soft, autonomous robots. *Nature* **2016**, *536*, 451−455.

(7) O'Bryan, C.; Bhattacharjee, T.; Niemi, S. R.; Balachandar, S.; Baldwin, N.; Ellison, S. E.; Taylor, C. R.; Sawyer, W. G.; Angelini, T. E. Three-dimensional printing with sacrificial materials for soft matter manufacturing. *MRS Bull.* **2017**, *42*, 571−577.

(8) Tokpavi, D. L.; Magnin, A.; Jay, P. Very slow flow of Bingham viscoplastic fluid around a circular cylinder. *J. Non-Newtonian Fluid Mech.* **2008**, *154*, 65−76.

(9) Mitsoulis, E. Flows of viscoplastic materials: models and computations. *Rheol. Rev.* **2007**, 137−158.

(10) Beris, A. N.; Tsamopoulos, J. A.; Armstrong, R. C.; Brown, R. A. Creeping motion of a sphere through a Bingham plastic. *J. Fluid Mech.* **1985**, *158*, 219.

(11) Deglo De Besses, B.; Magnin, A.; Jay, P. Viscoplastic flow around a cylinder in an infinite medium. *J. Non-Newtonian Fluid Mech.* **2003**, *115*, 27−49.

(12) Putz, A. M. V.; Burghelea, T. I.; Frigaard, I. A.; Martinez, D. M. Settling of an isolated spherical particle in a yield stress shear thinning fluid. *Phys. Fluids* **2008**, *20*, 033102.

(13) Gueslin, B.; Talini, L.; Herzhaft, B.; Peysson, Y.; Allain, C. Flow induced by a sphere settling in an aging yield-stress fluid. *Phys. Fluids* **2006**, *18*, 103101.

(14) Dinkgreve, M.; Denn, M. M.; Bonn, D. Everything flows?: elastic effects on startup flows of yield-stress fluids. *Rheol. Acta* **2017**, *56*, 189−194.

(15) Ma, T.; Yang, R.; Zheng, Z.; Song, Y. Rheology of fumed silica/polydimethylsiloxane suspensions. *J. Rheol.* **2017**, *61*, 205−215.

(16) Arigo, M. T.; McKinley, G. H. An experimental investigation of negative wakes behind spheres settling in a shear-thinning viscoelastic fluid. *Rheol. Acta* **1998**, *37*, 307−327.

(17) Kim, H.; Lee, J.; Kim, T.-H.; Kim, H.-Y. Spontaneous Marangoni mixing of miscible liquids at a liquid-liquid-air contact line. *Langmuir* **2015**, *31*, 8726−8731.

(18) Adrian, R. J.; Westerweel, J. *Particle Image Velocimetry*; Cambridge University Press: Cambridge, 2011.

(19) Santiago, J. G.; Wereley, S. T.; Meinhart, C. D.; Beebe, D. J.; Adrian, R. J. A particle image velocimetry system for microfluidics. *Exp. Fluid* **1998**, *25*, 316−319.